ISSN: 2161-0398

Journal of Physical Chemistry & Biophysics

Available online at: OMICS Publishing Group (www.omicsonline.org)

Physical Chemistry & Biophysics

Review Article   **Open Access**

AFM/TEM Complementary Structural Analysis of Surface-Functionalized Nanoparticles

Ruozi B[1]*, Belletti D[1], Vandelli MA[1], Pederzoli[1], Veratti[1], ...rni[1], ...osi[1], Tonelli M[2] and Zapparoli M[2]

[1]Department of Life Sciences, University of Modena and Reggio Emilia, Italy
[2]CIGS, Centro Interdipartimentale Grandi Strumenti, University of Modena and Reggio Emilia, Italy

Abstract

In the field of nanomedicine, the characterization of functionalized drug delivery systems, introduced on market as efficacious and selective therapeutics, represents a pivotal aspect of great importance. In particular, the morphology of polymeric nanoparticles, the most studied nanocarriers, is frequently assessed by transmission electron microscopy (TEM). Despite of TEM high resolution and versatility, this technology is frequently hampered by both the complicated procedure for sample preparation and the operative condition of analysis. Considering the scanning probe microscopies, atomic force microscopy (AFM) represents an extraordinary tool for the detailed characterization of submicron-size structure as the surface functionalization at the atomic scale. In this paper we discussed the advantage and limits of these microscopies applied to the characterization of PLGA nanoparticles functionalized with three different kinds of ligands (carbohydrate ligand, an antibody and quantum dots crystals) intentionally designed, created and tailored with specific physico-chemical properties to meet the needs of specific applications (targeting or imaging).

Graphical Abstract
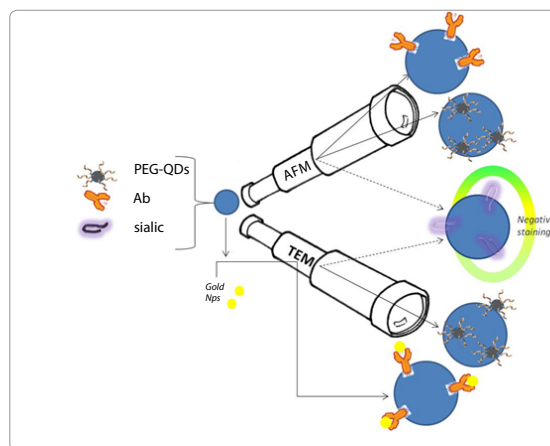
Keywords: Transmission electron microscopy (TEM); Atomic force microscopy (AFM); PLGA; Nanoparticles; Surface functionalization; Neu5Ac; Rituximab; Quantum Dots (QD)

Highlights

Short collection of bullet points of the core article

1. Nanomedicine deserves interesting perspective for real application in medicine and surface modified nanocarriers represent the cutting-edge of nanomedicine.

2. Aiming to the maximum translatability, surface-modified nanocarriers must be properly characterized, in terms of surface properties.

3. Advanced microscopies (Atomic Force Microscopy and Transmission Electron Microscopy) help in better understanding of the chemico-physical features of nanocarriers

4. AFM and TEM give high resolution outcomes and should be chosen depending on specific the nature of surface-ligands

5. AFM allows to discriminate on the qualitative evaluation of ligands of different nature (QDs vs antibody) , without any additional treatment and without operating in a vacuum environment

Introduction

In the pharmaceutical field, nanocarriers are designed to solve several limitations linked to the conventional forms of drug administration such the non-specific biodistribution of the drug, the lack of targeting towards specific cells or tissues, poor water solubility, low bioavailability, high toxicity and low therapeutic indices [1]. Particularly, polymeric nanoparticles (NPs) have been proposed both to stabilize and modulate the release of wide classes of drug (antibiotics, antitumorals, antifungines, vaccines etc) and, taking advantage of the formulative versatility of the carriers, to introduce new functions

*Corresponding author: Ruozi B, Department of Life Sciences, University of Modena and Reggio Emilia, Via Campi 183, 41124, Modena, Italy, Tel: +39.059.2055128; Fax: +39.0592055131; E-mail: barbara.ruozi@unimore.itac.

for targeting drugs and imaging agents [2,3]. In these contest, recent advances in the nanotechnology field are based on the functionalization of nanocarriers by incorporation, adsorption or conjugation of ligands (polymers, carbohydrates, antibodies, endogenous substances or markers) to their surface. The problems related to the characterization of nanocarriers and to the surface functionalization represent a major drawback to formulative developments. Moreover, the validity of some of the conclusions related to the quali-quantitative detection of the surface functionalization may be questionable although several analytical approaches have been proposed for characterizing the modified nanosystems, not leading to a standardized protocol and therefore comparable readouts. Nowadays, the most common techniques for the analysis of surface properties of functionalized nanocarriers are the zeta potential (ζ-pot) and the X-Ray analyses, particularly the Electron Spectroscopy for Chemical Analysis (ESCA). ζ-pot analysis is routinely used to define the surface charge of NPs and therefore the effects of the surface modification. Unfortunately, this approach does not allow to evaluate other properties such as the density and the homogeneity of the modification. Moreover, ζ-pot is accurately measured if the formulation satisfy several criteria such as its monodispersivity, low salt concentrations (conductivity <1 mS/cm), and the use of a particulate free polar dispersant as, for example, high purity water [4].

Like ζ-pot, the analysis of the chemical composition of the NPs surface by ESCA is often indicative of the presence of coating [5] but this qualitative detection does not clarify both the atomic surface arrangement and the local micro-structured occurred after surface functionalization. Details on the morphology, shape, macro- and microstructure characteristics of the NPs surface can be obtained by using a microscopical approach. Particularly the transmission electron microscopy (TEM) and the scanning probe microscopy (atomic force microscopy, AFM) are widely used to characterize nano- and atomic scale materials. TEM imaging has significantly higher resolution than the other microscopic procedures such as the light-based imaging technique. The nature of the substances and the preparation methods of the samples are extremely important in order to obtain high-quality images having the greatest contrast between NPs (or the surface details) and background.

The high resolution is also the most appealing advantage of AFM respect to other techniques such as electron microscopies (for example TEM). AFM allows 3D visualization and qualitative and quantitative information on native samples in physiological like conditions [6,7], avoiding complex sample preparation procedures and thus the connected artifacts.

Also in these cases, criticism should be addressed to detail the NPs surface. As example, the amplitude of forces involved and then the imaging mode to be adopted for the analysis should be appropriately set up on the nature of the samples [8].

Starting from these basis, this paper aims to define the preparative procedures of sample and the applicability of TEM and AFM techniques towards the evaluation of the surface details with sub-nanometer resolution in NPs modified by different kinds of ligands. To reach this aim, we prepared and analysed poly-lactide-co-glicolide (PLGA) NPs functionalized on the surface with ligands having different chemical nature and composition and capable to provide to the NPs physical-chemical properties required for specific application. We tested NPs engineered with a) a sialic acid derivative (Neu5Ac) direct against tumors (targeting aim) [9]; b) rituximab antibody recognized by B-chronic lymphocytic leukaemia cells (targeting aim) [10,11] and c)

quantum dots (QD) to obtain double imaging/drug release (theranostic aim). If compared with the encapsulation process, the conjugation and the exposure of QD on NPs surface is preferred in order to avoid the QD release and to ensure the optimal imaging [12,13].

Materials and Methods

Preparation of nanoparticles

All NPs analysed were obtained according to the nanoprecipitation procedure [14]. The functionalization can be inserted during NPs formulation by using polymer previously modified (Neu5Ac-PLGA502) or after the NPs formation by activating the functional groups onto NPs surfaces by *"in situ"* reaction and subsequent conjugation with ligands (Rituximab-PLGA503 NP and QD-PLGA503 NPs).

Sialic acid derivative conjugated nanoparticles (Neu5Ac-PLGA502 NPs) : Initially, PLGA502H (50% lactic/50% glycolic acid ratio, inherent viscosity 0.20 dl/g, MW 4900; Boehringer-Ingelheim, Ingelheim am Rhein, Germany), selected as polymer on the basis of the yield of sugar conjugation, was conjugated with Neu5Ac (Sigma Aldrich), a sialic acid derivative, by applying the protocols previously reported [15,16]. Then, a mixture composed by Neu5Ac-PLGA502 (5 % w/w) and PLGA502H (95% w/w) was dissolved in acetone (8 mL). The organic phase was then added dropwise into deionised water (25 mL) containing poloxamer 188 (Pluronic F68®, 100 mg) (Sigma Aldrich). After stirring at r.t. for 10 min, the organic solvent was removed at 30°C under reduced pressure (10 mmHg). The final volume of the suspension was adjusted to 10 mL with deionised water. The Neu5Ac-PLGA502 NPs were then purified by gel-filtration chromatography (Sepharose CL 4B gel (160 mL), column 50×2 cm, Sigma Aldrich, Italy), using water as the mobile phase. Un-modified PLGA502H NPs, prepared with the same experimental conditions but using only un-modified PLGA502H as the polymer, were considered as control samples. At least 3 batches of each NP sample were prepared.

Antibody conjugated nanoparticles (Rituximab-PLGA503 NPs): Rituximab (anti-human CD20 Ab-Mabthera; Roche, Basel, Switzerland) engineered NPs were prepared starting from un-modified PLGA503H NPs (50% lactic/50% glycolic acid ratio, inherent viscosity 0.38 dl/g, MW 11000; Boehringer-Ingelheim, Ingelheim am Rhein, Germany) applying the methodology previously described [17,18]. Briefly 50 mg of PLGA 503H NPs were reacted with 150 mg of 1-Ethyl-3-(3-dimethylaminopropyl)-carbodiimide (EDC; Sigma Aldrich, Saint Luis, MO) and 50 mg of N-Hydroxy-succinimide (NHS, Sigma Aldrich) in 0.1 M of 2-(N-morpholino) ethanesulfonic acid (MES, Sigma Aldrich) ethanesulfonic acid (MES, Sigma Aldrich) buffer (pH 4.7) and stirred at r.t. for 1 hour. EDC and NHS are used to activate carboxylic acid groups at the PLGA's nanoparticle surface, with formation of activated ester groups able to react with primary amino groups of the antibody. The activated NPs were collected by ultracentrifugation at 15, 000 rpm for 10 min at 4°C and the excess of reagents were removed. Activated NPs were re-suspended in PBS buffer pH 7.4 and stirred at r.t. for 1 hour with the designated volume of Rituximab (100 μL of a 1 mg/mL stock solution) in order to obtain Rituximab-PLGA503 NPs. After the reaction, the suspension of these engineered NPs were collected by centrifugation and further washed twice by distilled water. At least 3 batches of each NP sample were prepared.

QD conjugated nanoparticles (QD-PEG-PLGA503 NPs): PLGA503H NPs were previously obtained according to the nanoprecipitation technique by using as polymer PLGA503H and the 1% (w/v) of PVA acqueous solution as dispersing phase. The

NPs surface was activated via NHS/EDC as previously described for Rituximab-PLGA503 NPs (section 2.1.2.). The activated NPs were re-suspended in 4.5 mL of PBS pH 7.4. Then, 3 mL (corresponding to about 30 mg of NPs) of the NPs suspension were conjugated with 100 pmol of QD-PEG-NH$_2$ (Qdot605 ITK, Life technologies, Monza, Italy) to obtain QD-PEG-PLGA503 NPs. The reaction was allowed to carry out for 1 h at r.t.. Free QDs-PEG-NH$_2$ were removed by centrifugation and collected QD-PEG-PLGA503 NPs were re-suspended in deionized water. At least 3 batches of each NP sample were prepared.

Physico-chemical characterization of NPs

Photon correlation spectroscopy (PCS): All NPs were analyzed in distilled water for particle size (Z-average), polydispersivity index (PDI) and zeta potential (z-pot) by photon correlation spectroscopy (PCS) and laser Doppler anemometry using a Zetasizer Nano ZS (Malvern, UK; Laser 4 mW He–Ne, 633 nm, Laser attenuator Automatic, transmission 100% to 0.0003%, Detector Avalanche photodiode, Q.E >50% at 633 nm, t=25°C). The results were normalized with respect to a polystyrene standard solution. All the data are expressed as means of at least three determinations carried out for each preparation lot (three lots for each sample).

X-ray photoelectron spectroscopy (ESCA analysis): ESCA (Electron Spectroscopy for Chemical Analysis) is a surface-sensitive technique that measures the elemental composition and identifies the chemical functional groups in the 10 nm-thick surface layer of the sample. The composition of the surface layer of the Neu5Ac-PLGA502 NPs was determined from the detailed analysis of the C1s peak collected with a XRC 1000 X-ray source analysis system (Specs Surface Nano Analysis, Germany) and a Phoibos 150 hemispherical electron analyzer (Specs Surface Nano Analysis, Germany), using MgKα1,2 radiations. The spectra were recorded in FAT (fixed retardation ratio) mode with 190 eV pass energy. The pressure in the sample analysis chamber was about 10^{-10} Torr. Data acquisition was performed with the RBD AugerScan 2. High-resolution data were collected using a pass energy of 50 eV in 0.1 eV steps. Curve-fitting routines were performed with Igor Pro software. Signals were attributed as reported by Bondioli and coworkers (15).

ESCA was used also to quantify the presence of nitrogen atoms on the surface of Rituximab-PLGA503 NPs.

Transmission electron microscopy (TEM): A negative staining procedure was applied to observe the structure of both PLGA-502H NPs and Neu5Ac-PLGA502 NPs with TEM operating at an acceleration voltage of 200 KV (model JEM 2010; JEOL, Peabody, MA). To prepare particles for negative staining, a drop of a water-diluted suspension of the samples (about 0.05 mg/mL) was placed on a copper grid that was coated with a thin layer of carbon (TABB Laboratories Equipment, Berks, UK), allowed to adsorb and the surplus was removed by filter paper. Then, a drop of 2% (w/v) aqueous solution of uranyl acetate was applied to the sample for 5 min, and then wicked away; the concentration of uranyl acetate applied in this study was the most suitable to maintain the integrity of the sample during the preparation [19]. The sample was dried at room conditions before the NPs were imaged with a TEM.

Materials with electron densities that are significantly higher than amorphous carbon are easily imaged. These materials include most metals (e.g., silver, gold, copper, aluminum) and most oxides (e.g., silica, aluminum oxide, titanium oxide). Thus, in order to further assess the presence of Rituximab on the NPs surface, the Rituximab-
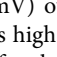
PLGA503 NPs were incubated with nanogold (mono-sulfo-N-Hydroxy-succinimido Nanogold®, Nanoprobes, Yaphank, NY, USA) (size 1.4 nm) able to react with Ab amine groups in order to provide a qualitative identification of Ab. As the control, we performed the same coupling reaction using PLGA503H NPs without Ab on the surface. Following the procedures given by the manufacturer, a weighted amount (1 mg) of lyophilized PLGA503H NPs or Rituximab-PLGA503 NPs were suspended in phosphate buffer (pH 7.8), added to 300 uL of a nanogold suspension (9 nmol) and adjusted to a final volume of 3 mL of solution. After purification, the NPs coupled with nanogold were placed on a copper grid coated with thin layer of carbon and processed for TEM analysis.

QD-PEG-PLGA503 NPs was observed without any treatment. The particle suspension was deposited on a copper grid and analysed. Elemental analysis of samples was also performed using TEM-Energy Dispersive X-ray Spectroscopy (EDS, Energy TEM INCA 300, Oxford Instruments, Halifax Road, Buckinghamshire HP12 35E, UK). In particular, in order to verify the presence of QDs on NPs, an arbitrarily chosen representative area of the sample was hit by primary beam electrons of TEM thus to produce X-rays that carry information as to the type of atoms (the elements) in the sample. Information about elemental composition and elemental weight % were displayed as a spectrum, identifying the present elements, by means of Oxford INCA 100 software.

Atomic force microscopy (AFM): Atomic force microscopy (AFM) was used to better clarify the morphology and the surface structure of the samples. The atomic force microscopical observations were performed with an Atomic Force Microscope (Park Instruments, Sunnyvale, CA, USA) at about 20°C operating in air and in *Non-Contact* (NC) mode using a commercial silicon tip-cantilever (high resolution noncontact "GOLDEN" Silicon Cantilevers NSG-11, NT-MDT, tip diameter=5–10 nm; Zelenograd, Moscow, Russia) with stiffness about 40 Nm^{-1} and a resonance frequency around 170 kHz. After the purification, the sample dispersed in distilled water were applied on a freshly cleaved mica disk (1 cm×1 cm); 2 min after the deposition, the water excess was removed using blotting paper. The AFM images were obtained with a scan rate 1 Hz and processed using a ProScan Data Acquisition software. Two kinds of images are obtained: the first one is a topographical image and the second one is indicated as "error signal". This error signal is obtained by comparing two signals: the first one, direct, representing the amplitude of the vibrations of the cantilever, and the other one being the amplitude of a reference point. The images obtained by this method show small superficial variations of the samples. Images were flattened using second-order fitting to remove [sample tilt] background curvature and slope from the images.

Results

Neu5Ac-PLGA502 NPs vs non functionalized PLGA502H NPs

The hydrodynamic diameters (Z-average) of the non-engineered PLGA502H NPs measured by PCS are around 170 nm and the size distributions are relatively narrow (polydispersity<0.1) Table 1. These NPs exhibit high negative value of ζ-pot (within -30 mV) owing to the exposure of carboxylic group of PLGA that indicates high electric charge on the surface of the NPs, which is responsible for the strong repulsive forces amongst the particles that prevents their aggregation in water and favors formation of stabilized NPs. The functionalization with Neu5Ac do not alter significantly the ζ-pot value of NPs.

ESCA analysis was used to identify the chemical composition of the NPs and try to investigate the effective presence of the sialic acid layer. C1s signal of the ESCA spectrum of the non-engineered PLGA502H NPs can be deconvoluted into three components see Table 1. Neu5Ac-PLGA502 NPs are characterized by an increase in the signal attributed to COO^- with respect to the non-engineered PLGA502H NPs. The increase of this signal could be due to the greater hydrophilicity of the Neu5Ac moiety respect to that of the carboxylic end of the polymer. This characteristic allows the placement of the sialic residue on the NPs surface during their preparation by nanoprecipitation.

Table 1: AFM and TEM images of PLGA502H NPs and Neu5Ac-PLGA502 NPs are shown in Figure 1. The images from negative-staining TEM and NC-AFM of NPs prepared using PLGA502H, revealed a population of homogeneous particles with a regular surface Figure 1, *panel a*. The size of particles obtained ranged from 100 to 200 nm. The range were consistent with the size obtained by PCS. At the same manner, the microscopical analysis of Neu5Ac-PLGA502 NPs demonstrated the formation of spherical particles, with delimited contour and reproducible coverage around 150 nm with a slightly increase of heterogeneity Figure 1, *panel b*.

Figure 1: TEM image contrast provided information on the structure of both PLGA502H NPs and Neu5Ac-PLGA502 NPs. Both systems can be considered as amorphous structures and then, the bright/dark contrast observed in TEM images can be ascribed to the Z number of atoms of components and to the thickness of the samples. Unfortunately, the same atoms (C, O, H) formed compositive polymer (PLGA502H) and sialic acid residue (Neu5Ac). Therefore, it is impossible to discriminate between the polymeric NPs and their surrounding layer. In fact, TEM microphotographs of Neu5Ac-PLGA502 NPs are similar as those of PLGA502H NPs. Also AFM experiments were unable to show the changes in surface topography of Neu5Ac-PLGA502 NPs respect to that of PLGA502HNPs.

Rituximab-PLGA503 NPs vs non functionalized PLGA503H NPs

A monomodal and monodisperse (PDI<0.1) distribution describes the PLGA503H NPs sample Table 2. The average hydrodynamic diameter (Z-average obtained by PCS analysis) of the NPs is ranged between 150 and 170 nm. The range is lower than that of engineered NPs on the surface with the Ab (Rituximab); Rituximab-PLGA503 NPs

show in fact a mean diameter larger than 200 nm, with a broader size distribution (PDI>0.2).

Table 2: PLGA503H NPs showed a negative ζ-pot value close to -25 mV; this value was due to the presence of free carboxyl groups of the polymer PLGA partially masked by residual PVA, still present also after purification being adsorbed on the surface of the NPs (estimated in a percentage of 5%). This hypothesis is supported by some previous studies showing that PLGA503H NPs prepared without PVA have a ζ-pot value of about -60 mV, while in the presence of PVA, the potential becomes less negative reaching values close to neutrality [20].

In the NPs engineered with the antibody, the ζ-pot values remained closed to -20 mV, but distributed in a wide range of values, confirming the presence of a more complex surface if compared with that of PLGA503H NPs.

Moreover, ESCA analysis, by investigating the presence of atoms (N) on the surface of Rituximab engineered NPs (Rituximab-PLGA503 NPs) could give proof of success of the surface engineering procedure Table 2. In fact, the atomic spectra of the engineered NPs (Rituximab-PLGA503 NPs) in comparison with that of non-engineered NPs (PLGA503H NPs) showed N signal indicating that the dislocation of Ab is on the NPs surface. The data indicated that the surface available for the interaction with the specific antigen can be approximately estimate to be about 7 ± 1% (percentage of derivatization).

TEM and AFM images of PLGA503H NPs described the defined and reproducible spherical morphology and smooth surface already observed for PLGA502H NPs (data not shown). Several differences were observed analyzing by TEM and AFM the Rituximab-PLGA503H NPs. To evaluate the presence of Ab on the NPs surface and in order to assess its reactivity, we set up a reaction of the Ab with gold NPs (Nanogold®) that appear well contrasted in the TEM microphotographs Figure 2. The images describe an heterogeneous population of NPs frequently connected by unformed material, probably due to residual reaction reagents not completely removed by the purification process, altering the NPs contours. Moreover the magnifications of TEM micrograph Figures 2, clearly shows the presence of nanosized objects (arrows) with a diameter close to 5 nm scattered on particle surface. This small, denser and darker objects on the NPs surface were reasonably ascribable to heavy elements [21,22]. The black spots, analyzed by EDS, used for elemental composition analysis, were described to be Au based

	PCS[a]			ESCA[b]		
				PLGA502H[c]	Surfactant (Pluronic)[c]	
Sample	Size[d] (nm)	PDI[e]	z-pot (mV)[d]	COO (1)[f] 290.5 eV	COO–C–O (2)[f] 288.5 eV	C–CH (3)[f] (overlapped to (4)[f]) 286.5 eV
PLGA502H NPs	171 (11)	0.09 (0.01)	−31 (2)	30.8	35.9	33.3
Neu5Ac-PLGA502 NPs	163 (5)	0.20 (0.02)	−37 (4)	36.0	35.4	28.6

[a]PCS: Photon Correlation Spectroscopy analyses
[b]ESCA: Electron Spectroscopy for Chemical Analysis
[c]Atomic composition and numbering of the components of PLGA502H NPs, PLGA and Pluronic.
[d]The values represent the means of at least three experiments; standard deviation in parentheses.
[e]PDI: polydispersity index.
[f]The numbers indicate the carbon atom type

Table 1: Chemico-physical characterization and ESCA analysis of PLGA502H NPs and Neu5Ac-PLGA502 NPs

Samples	PCS[a]			ESCA[b]			
	Size[c] (nm)	PDI[c,d]	z-pot (mV)[c]	O (%)	C (%)	N (%)	Deriv.(%)
PLGA503H NPs	160 (10)	0.05 (0.01)	-25 (2)	37.8 (0.8)	63.2 (0.9)		
Rituximab-PLGA503 NPs	223 (25)	0.21 (0.0)	-20 (7)	35.2 (.5)	62 (0.7)	1.4 (0.2)	( )

[a]PCS: Photon Correlation Spectroscopy analysis
[b]ESCA: Electron Spectroscopy for Chemical Analysis
[c]The values represent the means of at least three experiments; standard deviation in parentheses.
[d]PDI: polydispersity index.

Table 2: Chemico-physical characterization and ESCA analysis of PLGA503H NPs and Rituximab-PLGA50 NPs
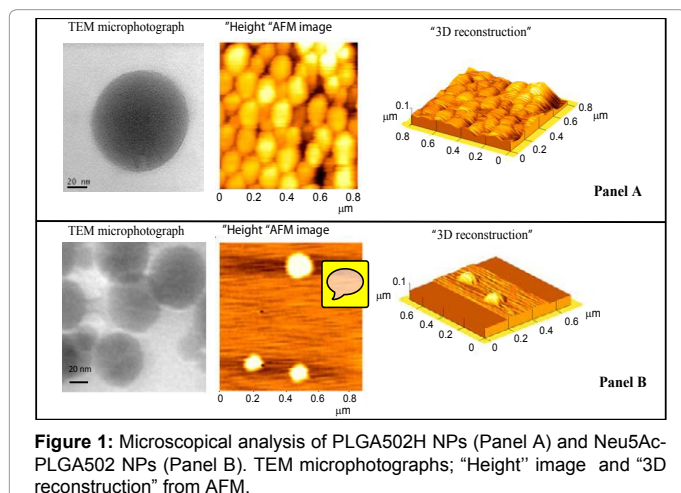

Figure 1: Microscopical analysis of PLGA502H NPs (Panel A) and Neu5Ac-PLGA502 NPs (Panel B). TEM microphotographs; "Height" image and "3D reconstruction" from AFM.

and therefore to be due to Nanogold® labelling and confirming the Ab molecules conjugated on the NPs surface Table 2

Figure 2: By using NC-AFM, surface alterations after conjugation with Rituximab appeared evident, without any preliminary preparative treatment of the samples. Structurally, Ab engineered NPs (Rituximab-PLGA503 NPs) were characterized by larger aggregates having irregular shapes. The analysis of the topographical images of the samples Figure 2 showed that, in accordance with the size measured by PCS analysis, the diameters of Rituximab-PLGA503 NPs were in a wide range (100-300 nm). The NPs were characterized by an irregular shape and fragmented contours. Additionally, the surface appeared characterized by the presence of grains not isolated any more, as already observed for similar systems [23,24]. The "Error signal" image and 3D reconstruction Figure 2 well detailed the surface of NPs where spherical structures with diameters of about 8–10 nm are present. This structure could be recognized as Ab molecules, as the images strongly agree with AFM images showing trimeric structures with comparable size of IgG [25]. Based on these results, AFM imaging appears particularly attractive to characterize particulate matter based on organic materials with high spatial resolution, such as Ab anchored on NPs surface, without any concern about scattering cross sections and sample treatment procedures.

QD-PEG-PLGA503 NPs vs non functionalized PLGA503H NPs

The QD-PEG-NH$_2$ used in this experiment are featured by a CdSe core encapsulated in a crystalline shell of ZnS and an external amphiphilic polymer coating to prevent formation of free Cd. The average particle size of CdSe/CdZnS QDs is approximately 26±1 nm as measured by PCS, probably due to aggregation phenomena. PCS analysis of QD-PEG-PLGA503 NPs were reported in Table 3. If compared with PLGA503H NPs, the Z-average of engineered QD-

PEG-PLGA503 NPs slightly increased from 160 ± 10 to 179 ± 13 nm. As the non-engineered NPs, QD-PEG-PLGA503-NPs appeared monomodal and uniformly distributed (0.09< PDI<0.13).

Table 3: The values of the ζ-pot appeared affected by the presence on the surface of QD-PEG-NH$_2$ chains. An increase in the surface charge for QD–PEG-PLGA503 NPs was occurred (−17 ± 2 mV) if compared with that of non-engineered PLGA503H NPs (−25 ± 2 mV). This difference in the ζ-pot is justified by literature data describing the ability of PEG polymer to mask the PLGA NPs surface, and particularly the exposed carboxyl group [26, 27].

Figure 3: We first observed QD-PEG-NH$_2$ by using TEM; based on contrasted images, we recognized and measured the size of the QD's core-shell (CdSe/ZnS) that was found around 7-8 nm Figure 3; to evaluate the entire QD-PEG-NH$_2$ we applied the AFM analysis Figure 3. By using this approach, we recognized the spherical formation of QD with a diameter ranging approximately from 20 nm to 25 nm Figure 3. These observations were in agreement with previous papers [28-30].

To visualize how the surface of PLGA503H NPs engineered with QDs, we analyzed the images captured by TEM Figure 4. Some of the NPs were still QD-free (data not shown), but in most of the evaluated cases some QDs were located on peripheral of NPs. QDs were scattered along the surface, confined in well located area with the tendency of the aggregation.

Energy Dispersive X-Ray using the EDS detector was used to map the QD-PEG-NH$_2$ based on their composition

Figure 4: PEG is composed mostly of carbon and oxygen, the same composition of PLGA polymer. PEG surrounding of Cd/Se core was not mapped. Unfortunately, the carbon signal with respect to the other signals was significantly larger diminishing the resolution of the smaller cadmium and selenium peaks, that appeared with a percentage close to 0.4% and <0.1%, respectively.

QD-PEG-PLGA503 NPs were easily visualized and characterized through AFM scanning, once the suspension was deposed on a mica

Sample	PCS[a]			EDS[b]
	Size[c] (nm)	PDI[c,d]	z-pot (mV)[c]	Cd vs C (%)
PLGA503H NPs	160 (10)	0.05 (0.01)	-25 (2)	
QD-PEG-NH$_2$	26 (1)	0.29 (0.01)	-21 (4)	
QD-PEG-PLGA503 NPs	179 (13)	0.11 (0.02)	-17 (2)	0.4 (0.02)

[a]PCS: Photon Correlation Spectroscopy analyses
[b]EDS: Energy dispersive X-ray Spectroscopy
[c]The values represent the means of at least three experiments; ±: standard deviation in parentheses.
[d]PDI: polydispersity index.

Table 3: Chemico-physical characterization and EDS analysis of PLGA503H NPs, QD-PEG-NH$_2$ and QD-PEG-PLGA503 NPs

Figure 2: Microscopical analysis of Rituximab-PLGA503 NPs. Microphotograph and magnifications from TEM; "Height" image, "Error signal" image and 3D reconstruction from AFM.

Figure 3: Microscopical analysis of QD-PEG-NH2. TEM microphotographs; "Height" image, "Height" profile elaboration and 3D reconstruction from AFM.

Figure 4: Microscopical analysis of QD-PLGA503 NPs. Microphotograph, magnification, and EDS analysis from TEM; "Height", "Error signal" and 3D reconstruction from AFM.

support. AFM topography images of QD-PEG-PLGA503 NPs sample deposited on mica demonstrate the presence of spherical flattened particles quite polydisperse with a mean diameter of about 230 nm Figure 4. Interestingly, the height AFM image showed that the conjugation of QD with NPs does not result in a regular surface, but rather in a discontinuous rough one. This was in sharp contrast with the control NPs showing a smooth surface. Also 3D image analysis indicated that QD were randomly distributed the surface of NPs, forming visible agglomerates Figure 4. Moreover, the adsorption/conjugation of QD-PEG-NH$_2$ molecules on the NPs surface, reducing the net charge as demonstrated also by ζ-pot analysis, could promote the formation of aggregates and flattened species among the NPs. The occurrence of these destabilization might be strongly reduced in suspension samples for the presence of solvatation interactions, but they are predominant in solid state and therefore they can strongly affect the chemical-physical behavior of the samples. As evident, AFM is one of the few methods which allows one to visualize the formation of these assemblies.

Conclusions

This study demonstrates that AFM and TEM are really representing good options to be able to discriminate amongst the ligands conjugated on the NP surface. These technologies would be really useful especially in the view of the upcoming era of surface engineered nanomedicines. In fact, there is need for a precise, clear and accurate characterization of active surface of these new smart carriers.

Advance surface-analysis technologies should be chosen in function of the ligands/molecules used for surface engineered of nanomedicines.

In this view, in this paper, we showed that TEM and AFM can work together, giving at the same time different information of different nature, converging to draw a more and precise "picture" of the novel nanomedicine.

Without any staining or macromolecules labeling (like metallic nanogold) the TEM detection of organic molecules using as ligand (such as carbohydrate or antibody)composed by the same element of the matricial structure of nanoparticles, is difficult. In particular, we showed that despite the high resolution of the two microscopical techniques, low molecular weight molecules, such as sugar residues (Neu5Ac), anchored to the surface of polymeric NPs were not detectable both with TEM and AFM.

QD, that are materials with electron densities significantly higher than amorphous carbon are easily imaged by using TEM, but also detectable by AFM approach without any additional treatment of the samples and without operating in a vacuum environment.

As support of our conclusion, we detected by TEM the presence of antibody, a complex high molecular weight ligand, on nanoparticles surface only by introducing Nanogold® labeling. Also in this case, AFM allowed to discriminate on the qualitative evaluation of antibody, without any preparative treatment of the sample.

Moreover, AFM images shows 3D-data allowing the height of the observed object to be measured as well as the heterogeneity/discontinuity of the coverage or the surface alteration occurred during the functionalization of NPs to be defined. Hence, AFM can support additional analytical techniques allowing the sample characterization as detailed as possible.

References

1. Webster DM, Sundaram P, Byrne ME (2013) Injectable nanomaterials for drug delivery: carriers, targeting moieties, and therapeutics. Eur J Pharm Biopharm 84: 1-20.

2. Feng L, Zhu C, Yuan H, Liu L, Lv F, et al. (2013) Conjugated polymer nanoparticles: preparation, properties, functionalization and biological applications. Chem Soc Rev 42: 6620-6633.

3. Rhyner MN, Smith AM, Gao X, Mao H, Yang L, et al. (2006) Quantum dots and multifunctional nanoparticles: new contrast agents for tumor imaging. Nanomedicine (Lond) 1: 209-217.

4. PC, Lin S, Wang RS (2013) Biotechnol Adv pii: S0734-9750(13) 00211-215.

5. Lemarchand C, Gref R, Couvreur P (2004) Polysaccharide-decorated nanoparticles. Eur J Pharm Biopharm 58: 327-341.

6. B Drake, CB Prater, AL Weisenhorn, SA Gould, TR Albrecht, et al. (1989) Imaging crystals, polymers, and processes in water with the atomic force microscopeScience 243: 1586-1589.

7. Bustamante C, Rivetti C, Keller DJ (1997) Scanning force microscopy under aqueous solutions. Curr Opin Struct Biol 7: 709-716.

8. aalousha M, Lead JR (2013) Colloids and Surfaces A: Physicochem. Eng Aspects 419: 238–247

9. Jayant S, Khandare JJ, Wang Y, Singh AP, Vorsa N, et al. (2007) Targeted sialic acid-doxorubicin prodrugs for intracellular delivery and cancer treatment. Pharm Res 24: 2120-2130.

10. Mukerjee A, Ranjan AP, Vishwanatha JK (2012) Combinatorial nanoparticles for cancer diagnosis and therapy. Curr Med Chem 19: 3714-3721.

11. Jaglowski SM, Byrd JC (2010) Rituximab in chronic lymphocytic leukemia. Semin Hematol 47: 156-169.

12. Cheng FY, Wang SP, Su CH, Tsai TL, Wu PC, et al. (2008) Stabilizer-free poly(lactide-co-glycolide) nanoparticles for multimodal biomedical probes. Biomaterials 29: 2104-2112.

13. Wen-Shuo Kuo,Shiaw-Min Hwang,Hei-Tin Sei,Yu-Cian Ku,Lee-Feng Hsu, et al. (2009) Stabilizer-Free Poly(lactide-co-glycolide) Nanoparticles Conjugated with Quantum Dots as a Potential Carrier Applied in Human Mesenchymal Stem Cells. Chem Soc 56: 940-948.

14. Fessi H, Puisieux F, Devissaguet JP, Ammoury N, Benita S (1989) Nanocapsule formation by interfacial polymer depositionfollowing solvent displacementInt J Pharm 55: R1–R4.

15. Bondioli L, Costantino L, Ballestrazzi A, Lucchesi D, Boraschi D, et al. (2010) PLGA nanoparticles surface decorated with the sialic acid, N-acetylneuraminic acid. Biomaterials 31: 3395-3403.

16. Vergoni AV, Tosi G, Tacchi R, Vandelli MA, Bertolini A, et al. (2009) Nanoparticles as drug delivery agents specific for CNS: in vivo biodistribution. Nanomedicine 5: 369-377.

17. Nobs L, Buchegger F, Gurny R, Allémann E (2003) Surface modification of poly(lactic acid) nanoparticles by covalent attachment of thiol groups by means of three methods. Int J Pharm 250: 327-337.

18. Nobs L, Buchegger F, Gurny R, Allémann E (2004) Poly(lactic acid) nanoparticles labeled with biologically active Neutravidin for active targeting. Eur J Pharm Biopharm 58: 483-490.

19. Ruozi B, Belletti D, Tombesi A, Tosi G, Bondioli L, et al. (2011) AFM, ESEM, TEM, and CLSM in liposomal characterization: a comparative study. Int J Nanomedicine 6: 557-563.

20. Costantino L, Gandolfi F, Bossy-Nobs L, Tosi G, Gurny R, et al. (2006) Nanoparticulate drug carriers based on hybrid poly(D,L-lactide-co-glycolide)-dendron structures. Biomaterials 27: 4635-4645.

21. Belletti D, Tonelli M, Forni F, Tosi G, Vandelli MA, uoza 3) Colloids and Surfaces A: Physicochem. Eng Aspects 436: 459-466

22. Egerton R (2005) Physical Principles of Electron Microscopy: An Introduction to TEM, SEM, and AEM. Springer: 1-214

23. Vilella A, Tosi G, Grabrucker AM, Ruozi B, Belletti D, et al. (2014) Insight on the fate of CNS-targeted nanoparticles. Part I: Rab5-dependent cell-specific uptake and distribution. J Control Release 174: 195-201.

24. Tosi G, Vilella A, Chhabra R, Schmeisser MJ, Boeckers TM, et al. (1997) Insight on the fate of CNS-targeted nanoparticles. Part II: Intercellular neuronal cell-to-cell transportJ Control Release 177, (2014), 96-107.

25. ritz, D. Anselmetti, J. Jarchow, X Fe nàndez-Busquet truct Biol 119: 165–171.

26. Kouchakzadeh H, Shojaosadati SA, Maghsoudi A, Vasheghani Farahani E (2010) Optimization of PEGylation conditions for BSA nanoparticles using response surface methodology. AAPS PharmSciTech 11: 1206-1211.

27. Ya-Ping Lia, b,Yuan-Ying Peia, Xian-Ying Zhangb, Zhou-Hui Gub,Zhao-Hui Zhou, et al. (2001) PEGylated PLGA nanoparticles as protein carriers: synthesis, preparation and biodistribution in ratsJ Control Release 71: 203-211.

28. Smith AM, Duan H, Mohs AM, Nie S (2008) Bioconjugated quantum dots for in vivo molecular and cellular imaging. Adv Drug Deliv Rev 60: 1226-1240.

29. Pellegrino T, Manna L, Kudera S, Lied T, Koktysh D, . (2004) Hydrophobic Nanocrystals Coated with an Amphiphilic Polymer Shell: A General Route to Water Soluble Nanocrystals. Nano Lett 4: 703–707

30. Feugang JM, Youngblood RC, Green M, Fahad AS, Monroe WA, et al. (2012) Nanobiotechnology 10: 45-52.